Neurochemistry International 122 (2019) 19–30

Contents lists available at ScienceDirect

Neurochemistry International

journal homepage: www.elsevier.com/locate/neuint

Protein disulfide-isomerase A3 significantly reduces ischemia-induced damage by reducing oxidative and endoplasmic reticulum stress

Dae Young Yoo[a,b,1], Su Bin Cho[c,1], Hyo Young Jung[a], Woosuk Kim[a], Kwon Young Lee[d], Jong Whi Kim[a], Seung Myung Moon[e,f], Moo-Ho Won[g], Jung Hoon Choi[d], Yeo Sung Yoon[a], Dae Won Kim[h], Soo Young Choi[c,*], In Koo Hwang[a,**]

[a] Department of Anatomy and Cell Biology, College of Veterinary Medicine, Research Institute for Veterinary Science, Seoul National University, Seoul, 08826, South Korea
[b] Department of Anatomy, College of Medicine, Soonchunhyang University, Cheonan, Chungcheongnam, 31151, South Korea
[c] Department of Biomedical Sciences, Research Institute for Bioscience and Biotechnology, Hallym University, Chuncheon, 24252, South Korea
[d] Department of Anatomy, College of Veterinary Medicine and Institute of Veterinary Science, Kangwon National University, Chuncheon, 24341, South Korea
[e] Department of Neurosurgery, Dongtan Sacred Heart Hospital, College of Medicine, Hallym University, Hwaseong, 18450, South Korea
[f] Research Institute for Complementary & Alternative Medicine, Hallym University, Chuncheon, 24253, South Korea
[g] Department of Neurobiology, School of Medicine, Kangwon National University, Chuncheon, 24341, South Korea
[h] Department of Biochemistry and Molecular Biology, Research Institute of Oral Sciences, College of Dentistry, Gangneung-Wonju National University, Gangneung, 25457, South Korea

ARTICLE INFO

Keywords:
Protein disulfide-isomerase A3
Hippocampus
Gerbil
Oxidative stress
Tat peptide
Endoplasmic reticulum stress

ABSTRACT

Ischemia causes oxidative stress in the endoplasmic reticulum (ER), accelerates the accumulation of unfolded and misfolded proteins, and may ultimately lead to neuronal cell apoptosis. In the present study, we investigated the effects of protein disulfide-isomerase A3 (PDIA3), an ER-resident chaperone that catalyzes disulfide-bond formation in a subset of glycoproteins, against oxidative damage in the hypoxic HT22 cell line and against ischemic damage in the gerbil hippocampus. We also confirmed the neuroprotective effects of PDIA3 by using PDIA3-knockout HAP1 cells. The HT22 and HAP1 cell lines showed effective (dose-dependent and time-dependent) penetration and stable expression of the Tat-PDIA3 fusion protein 24 h after Tat-PDIA3 treatment compared to that in the control-PDIA3-treated group. We observed that the fluorescence for both 2′,7′-dichlorofluorescein diacetate (DCF-DA) and terminal deoxynucleotidyl transferase dUTP nick-end labeling (TUNEL), which are markers for the formation of hydrogen peroxide (H_2O_2)-induced reactive oxygen species and apoptosis, respectively, was higher in HAP1 cells than in HT22 cells. The administration of Tat-PDIA3 significantly reduced the (1) DCF-DA and TUNEL fluorescence in HT22 and HAP1 cells, (2) ischemia-induced hyperactivity that was observed 1 day after ischemia/reperfusion, (3) ischemia-induced neuronal damage and glial (astrocytes and microglia) activation that was observed in the hippocampal CA1 region 4 days after ischemia/reperfusion, and (4) lipid peroxidation and nitric oxide generation in the hippocampal homogenates 3–12 h after ischemia/reperfusion. Transient forebrain ischemia significantly elevated the immunoglobulin-binding protein (BiP) and C/EBP-homologous protein (CHOP) mRNA levels in the hippocampus at 12 h and 4 days after ischemia, relative to those in the time-matched sham-operated group. Administration of Tat-PDIA3 ameliorated the ischemia-induced upregulation of BiP mRNA levels versus the Tat peptide- or control-PDIA3-treated groups, and significantly reduced the induction of CHOP mRNA levels, at 12 h or 4 days after ischemia. Collectively, these results suggest that Tat-PDIA3 acts as a neuroprotective agent against ischemia by attenuating oxidative damage and blocking the apoptotic pathway that is related to the unfolded protein response in the ER.

1. Introduction

The transient interruption of blood flow to the brain decreases the oxygen and glucose supply to neurons, causing neuronal damage, especially in vulnerable regions such as the hippocampus. Although numerous underlying mechanisms for this neuronal damage have been

* Corresponding author.
** Corresponding author.
E-mail addresses: sychoi@hallym.ac.kr (S.Y. Choi), vetmed2@snu.ac.kr (I.K. Hwang).
[1] Dae Young Yoo and Su Bin Cho are equally contributed to this article.

https://doi.org/10.1016/j.neuint.2018.11.002
Received 6 August 2018; Received in revised form 2 November 2018; Accepted 2 November 2018
Available online 03 November 2018
0197-0186/

proposed, the mechanism of focus herein is the accumulation of unfolded or misfolded proteins during endoplasmic reticulum (ER) stress in neurons after ischemia/reperfusion (Kumar et al., 2003; Tajiri et al., 2004). In the normal state, neurons adequately perform the protein-folding process in the ER, and then the folded proteins exit the ER, whereupon they are relocated to their respective destinations. Under abnormal states, the expression of ER-resident chaperones compensates for the protein misfolding (Kozutsumi et al., 1988). However, in chronic neurodegenerative diseases, the ER-resident chaperones can alter ER function, leading to the abnormal accumulation of misfolded proteins (Kaufman, 2002). It is known that ER stress can cause cells to activate adaptive processes via the unfolded protein response (UPR) that help to restore normal ER function. In the normal state, immunoglobulin-binding protein (BiP), an ER chaperone, is bound to the ER stress sensors; however, BiP becomes dissociated from the ER sensors under abnormal condition and binds to the misfolded proteins as they accumulate (Rutkowski et al., 2006). As such, BiP facilitates proper protein folding and inhibits protein aggregation, while C/EBP-homologous protein (CHOP), a transcription factor induced by ER stress, increases pro-apoptotic pathway components, such as those of the BCL-2 protein family, and thus induces apoptosis (Oyadomari and Mori, 2004).

Several lines of evidence demonstrate that protein disulfide isomerase (PDI) likely functions as an efficient terminator of native oxidative protein folding with redox-dependent rearrangement of its thioredoxin-like domains (Serve et al., 2010; Wang et al., 2013). PDI, an ER-resident chaperone and a key UPR-induced chaperone, has diverse and conflicting functions in various animal models and systems; in fact, *PDI* is one of the major target genes induced by the UPR transcriptional program (Matus et al., 2013). Generally, PDI is used for the PDIA1 gene/protein as well as for the protein family including PDIA1 and PDIA3. For instance, PDI and PDIA3 can display Bak-dependent, pro-apoptotic activity via permeabilization of the mitochondrial outer membrane (Zhao et al., 2015a). Recently, research has shown that PDIA3 is a potential candidate as an alternate membrane-associated receptor that binds 1,25-dihydroxy-vitamin D3, which can regulate bone formation and apoptosis (Sohn et al., 2016). Indeed, PDIA3 heterozygous mice show severe osteoblastic disorders characterized by reduced growth plates and bone mass (Doroudi et al., 2014; Yuan et al., 2017b). However, the brain displays an increase in PDI following hypoxia or ischemia and these increases may be associated with compensatory mechanisms to reduce the neuronal damage after hypoxia or ischemia (Hwang et al., 2005; Nomura, 2004; Tanaka et al., 2000; Truettner et al., 2009). In addition, a heart-failure model revealed that the *PDI* gene is upregulated in the viable, peri-infarct myocardial region within the first few days following infarction, while a postmortem model revealed an inverse correlation between the expression of PDI and the apoptotic rate (Cominacini et al., 2015). Another recent study demonstrated that the overexpression of PDI attenuates the ubiquitination of proteins and decreases the activation of pro-apoptotic caspases in the SH-SY5Y cell line from human neuroblast from neural tissue (Liu et al., 2015). Further, PDI transgenic animals display protective effects against sciatic nerve damage and enhanced locomotor recovery after mechanical injury of sciatic nerve (Castillo et al., 2015). In a previous study, we demonstrated that transient spinal cord ischemia significantly changes the PDIA3 protein expression levels, and, using a proteomic approach, we showed that PDIA3 may serve as a therapeutic agent against ischemic damage in the spinal cord (Yoo et al., 2017). Nevertheless, few reports have illustrated the neuroprotective properties of PDIA3 against ischemic damage in animal models or hippocampal cell lines.

In the central nervous system, the blood-brain barrier and poor cytoplasmic delivery can hinder the expected effects of bioactive compounds on targets. Accumulating evidence suggests that the protein transduction domain effectively facilitates the intracellular delivery of proteins and synthetic drugs (Srimanee et al., 2015). Tat protein of human immunodeficiency virus type 1 is widely used to deliver different molecules into cells without any cellular toxicity. Tat protein transduction domain can form transient pores and translocate across the membranes by diffusing on these pores, on account of the strong electrostatic attraction between positively-charged Tat and negatively charged phospholipid (Chen et al., 2013b; Song et al., 2015). In previous studies, we demonstrated efficient delivery of Tat-reporter fusion protein to the hippocampus after intraperitoneal injection the protein (Eum et al., 2004) and significantly reduced ischemic insult-induced neuronal damage following treatment with the Tat peptide and other proteins with therapeutic action (Eum et al., 2004; Kim et al., 2015).

In the present study, we investigated the roles of Tat-PDIA3 on hydrogen peroxide (H_2O_2)-induced neuronal damage in the HT22 mouse hippocampal cell line and ischemia-induced neuronal damage in the gerbil hippocampus. We selected the hippocampus because it is easier to detect cell death and its related mechanisms in this region and because it shows less-severe neuronal damage than other regions affected by middle cerebral artery occlusion-induced focal ischemia. To confirm the roles of PDIA3, we also employed near-haploid PDIA3 knockout cells and observed the effects of Tat-PDIA3 on hydrogen peroxide (H_2O_2)-induced neuronal damage in the HT22 mouse hippocampal cell line.

2. Materials and methods

2.1. Cell preparation

The HT22 murine hippocampal neuronal cells were cultured in Dulbecco's modified Eagle's medium supplemented with 10% fetal bovine serum and antibiotics at 37 °C under humidified conditions of 95% air and 5% CO_2. The near-haploid PDIA3 knockout cell line was purchased from Horizon Genomics GmbH (Vienna, Austria). PDIA3 knockout cells were made with CRISPR/Cas9 edition in exon 3 with 8 bp mutation from HAP1 cells, which is a near-haploid cells derived from male chronic myelogenous leukemia cell line (Carette et al., 2011). HT22 and PDIA3 knockout HAP1 cells were plated in multiple-well plates at 2×10^6 cells/cm^2 and used for further study.

2.2. Construction of expression vectors

A Tat expression vector was prepared as described in a previous study (Kim et al., 2015). To construct the Tat-PDIA3 protein, PDIA3 cDNA was amplified by polymerase chain reaction (PCR) with the following primers: sense primer 5′-CTCGAGATGCGCCTCCGC-3′ and antisense primer 5′-GGATCCTTAGAGATCCTCCTGTGCC-3′. This PCR product was subcloned in a TA cloning vector and ligated with a Tat expression vector. A PDIA3 expression vector without the Tat protein transduction domain was constructed for use as a control.

The Tat-PDIA3 and control-PDIA3 plasmids were expressed in *Escherichia coli* BL21 treated with 0.1 mM isopropyl-β-d-thiogalactoside (Duchefa, Haarlem, Netherlands) at 18 °C for 8 h and purified using a Ni^{2+}-nitrilotriacetic acid Sepharose affinity column and PD-10 column chromatography (Amersham, Braunschweig, Germany). Endotoxins in the purified proteins were eliminated using Detoxi-Gel™ endotoxin removing gel (Pierce, Rockford, IL, USA). Endotoxin levels in the purified proteins were below the detection limit (< 0.1 EU/mL) when tested using a Limulus amoebocyte lysate assay (BioWhittaker, Walkersville, MD, USA). The concentration of purified Tat-PDIA3 and control-PDIA3 proteins was estimated by the Bradford assay (Bradford, 1976).

2.3. Transduction of Tat-PDI3A proteins into HT22 and PDIA3 knockout cells

We treated HT22 and PDIA3 knockout cells with different concentrations (0.5–3 μM) of Tat-PDIA3 protein and control-PDIA3 protein for 1 h and with 3 μM of both proteins for various durations (15–60 min) to examine the concentration-dependent and time-

dependent transduction abilities of Tat-PDIA3 protein, respectively. The cells were then treated with trypsin-ethylenediaminetetraacetic acid for 10 min and washed with phosphate-buffered saline (PBS) to eliminate proteins attached to the cellular membranes. Cells were lysed with ice-cold radioimmunoprecipitation assay buffer (Thermo Scientific, IL, USA) and the lysates were centrifuged at 13,000 × *g* for 20 min at 4 °C. The protein concentration of the supernatant was quantified by the Bradford assay (Bradford, 1976). Equal amounts of the proteins were separated by sodium dodecyl sulfate polyacrylamide gel electrophoresis (SDS-PAGE) and analyzed with western blots using a rabbit anti-histidine primary antibody (1:2000; Santa Cruz Biotechnology, Santa Cruz, CA, USA) and a goat anti-rabbit secondary antibody (1:5000; Santa Cruz Biotechnology).

2.4. Confocal fluorescence microscopy

The intracellular distribution of transduced Tat-PDIA3 protein in HT22 and PDIA3 knockout cells was observed by confocal fluorescence microscopy, as described previously (Jeong et al., 2014; Shin et al., 2014). Culture medium was placed on coverslips and treated with 3 μM Tat-PDIA3 protein. After 1 h of incubation at 37 °C, cells were washed twice with PBS and fixed with 4% paraformaldehyde for 5 min. The cells were treated with PBS containing 3% bovine serum albumin and 0.1% Triton X-100 (PBS-BT) at 25 °C for 30 min, and washed with the same solution. The cells were incubated at 25 °C for 4 h with primary antibody (1:2000; His-probe, Santa Cruz Biotechnology) followed by incubation in the dark for 1 h with the secondary antibody (1:1500; Alexa Fluor 488; Invitrogen, Carlsbad, CA, USA). To detect the intracellular ER localization of transduced Tat-PDIA3 protein in HT22 cells, the cells were incubated at 25 °C for 4 h with a mixture of His-probe antibody (1:2000; Santa Cruz Biotechnology) and KDEL ER marker (1:50; 10C3 clone; Santa Cruz Biotechnology). Thereafter, the cells were incubated in the dark for 1 h with a mixture of the Alexa Fluor 488-conjugated goat anti-rabbit IgG (1:1500; Invitrogen) and Alexa Fluor 594-conjugated anti-mouse IgG (1:1500, Invitrogen). Nuclei were stained with 1 μg/mL 4′,6-diamidino-2-phenylindole (DAPI; Roche Applied Science, Mannheim, Germany) for 2 min. A confocal fluorescence microscope confocal laser-scanning system (LSM 510 META NLO; Zeiss GmbH, Jena, Germany) was used to image the stained cells.

2.5. Assessment of cell viability and DNA damage

The biological activity of Tat-PDIA3 protein was measured by assessing cell viability using a WST-1 assay kit (Daeillab Service, Seoul, South Korea) after exposure to H_2O_2, as previously described (Jeong et al., 2014; Shin et al., 2014) and shown in Fig. 2A. The HT22 and PDIA3 knockout cells, plated at a confluence of 70% in a 96-well plate, were exposed to the Tat peptide, control-PDIA3, or Tat-PDIA3 proteins (0.5–3 μM). Following a 1-h incubation after exposure to the Tat peptide, control-PDIA3, or Tat-PDIA3 proteins, cells were treated with 1 mM H_2O_2 and incubated for 5 h. Cell viability was measured at 450 nm using an enzyme-linked immunosorbent assay (ELISA) microplate reader (Labsystems Multiskan MCC/340, Helsinki, Finland) and expressed as a percentage of untreated control cells.

To examine whether transduced Tat-PDIA3 proteins protect against DNA damage in H_2O_2-treated cells, HT22 and PDIA3 knockout cells were pre-treated with 3 μM Tat-PDI3A and control-PDIA3 protein for 1 h and exposed to 1 mM H_2O_2 for 3 h. Terminal deoxynucleotidyl transferase-mediated biotinylated dUTP nick end labeling (TUNEL) and a Cell Death Detection kit (Roche Applied Science) were used to assess cellular damage. Images were obtained using a fluorescence microscope (Nikon eclipse 80i, Tokyo, Japan) (Shin et al., 2014). Fluorescence was measured using a Fluoroskan ELISA plate reader (Labsystems Oy) at 485 nm excitation and 538 nm emission.

2.6. Measurement of intracellular reactive oxygen species levels

Intracellular reactive oxygen species (ROS) levels were measured using 2′,7′-dichlorofluorescein diacetate (DCF-DA), which converts to fluorescent DCF in cells when exposed to ROS, as described previously (Kim et al., 2015; Shin et al., 2014). The ROS levels in HT22 and PDIA3 knockout cells were determined in the presence or absence of Tat-PDIA3 protein (0.5–3 μM). After 1 h of pre-treatment with Tat-PDIA3 protein, the cells were treated with H_2O_2 (1 mM) for 10 min. Following a PBS wash, the cells were treated with 20 μM DCF-DA for 30 min. Fluorescence levels were measured using a Fluoroskan ELISA plate reader (Labsystems Oy) at 485 nm excitation and 538 nm emission.

2.7. Experimental animals

Male gerbils (3 months old, 50–60 g) were purchased from Japan SLC Inc. (Shizuoka, Japan). They were housed under standard conditions with adequate temperature (22 ± 2 °C) and humidity (60 ± 5%) control and a 12:12 h light/dark cycle with *ad libitum* access to food and water. The handling and care of the animals conformed to guidelines of current international laws and policies (National Institutes of Health Guide for the Care and Use of Laboratory Animals, Publication No. 85–23, 1985, revised 1996). The Institutional Animal Care and Use Committee of Seoul National University approved the animal procedures (SNU-160304-3). All experiments were conducted with an effort to minimize the number of animals used and the physiological stress caused by the procedures employed. All experimental procedures were conducted according to ARRIVE guidelines (Kilkenny et al., 2010).

2.8. Induction of transient forebrain ischemia

The animals were anesthetized with a mixture of 2.5% isoflurane (Baxtor, Deerfield, IL, USA) in 33% oxygen and 67% nitrous oxide. Common carotid arteries were isolated and occluded bilaterally using non-traumatic aneurysm clips, as described previously (Jung et al., 2018). Complete interruption of blood flow was confirmed by observing the central artery in the retinae using an ophthalmoscope (HEINE K180®; Heine Optotechnik, Herrsching, Germany). After 5 min of occlusion, the aneurysm clips were removed. Body temperature under free-regulating or normothermic (37 ± 0.5 °C) conditions was monitored with a rectal temperature probe (TR-100; Fine Science Tools, Foster City, CA, USA) and maintained using a thermometric blanket before, during, and after surgery, until the animals completely recovered from anesthesia. Thereafter, animals were housed in a thermal incubator (Mirae Medical Industry, Seoul, South Korea) to maintain their body temperature until the animals were euthanized. Five animals were excluded due to incomplete occlusion of the common carotid arteries and uncontrolled body temperature. Sham-operated animals were subjected to the same surgical procedures except that the common carotid arteries were not occluded.

2.9. Spontaneous motor activity

To check the effects of Tat-PDIA3 on hyperactivity after ischemic damage, the spontaneous motor activity of the gerbils was measured 1 day before and after the ischemia/reperfusion, as described previously (Yoo et al., 2015). The gerbils were individually placed in a Plexiglas cage (25 cm × 20 cm × 12 cm) within a soundproof chamber. A Photobeam Activity System-Home Cage (San Diego Instruments) was used to record locomotor activity. Spontaneous motor activity was monitored for 60 min. Scores were generated from live observations, and video sequences were used for subsequent re-analysis.

2.10. Tissue processing

The animals in the sham-operated group and ischemia-operated

groups, which included the Tat peptide-treated, control-PDIA3-treated, and Tat-PDIA3-treated groups ($n = 5$ in each group), were anesthetized with 1 g/kg urethane (Sigma-Aldrich, St. Louis, MO, USA) 4 days after ischemia/reperfusion. They were then perfused transcardially with 0.1 M PBS (pH 7.4) followed by 4% paraformaldehyde in 0.1 M phosphate-buffer (pH 7.4), as described previously (Jeong et al., 2014; Jung et al., 2018; Yoo et al., 2015). The brains were dissected out and post-fixed for 12 h in the same fixative. The brain tissues were cryoprotected by overnight infiltration with 30% sucrose. Serial brain sections were cut in the coronal plane at a thickness of 30 μm using a cryostat (Leica, Wetzlar, Germany) and collected in 6-well plates containing PBS for further processing.

The sections were processed under the same conditions to ensure that the immunohistochemical data were comparable among the groups. Tissue sections between 1.4 and 2.0 mm posterior to the bregma, in reference to a gerbil atlas (Loskota et al., 1974), were selected for each animal. Five sections, separated by 90-μm intervals, were sequentially treated with 0.3% H_2O_2 in PBS for 30 min and 10% normal goat serum in 0.05 M PBS for 30 min at 25 °C. Sections first underwent an overnight incubation with mouse anti-neuronal nuclei (NeuN) antibody (1:1000; Milipore, Temecula, CA, USA), rabbit anti-glial fibrillary acidic protein (GFAP; 1:1000; Milipore), or rabbit anti-ionized calcium-binding adapter molecule 1 (Iba-1; 1:500; Wako, Osaka, Japan) at 25 °C. Thereafter, the sections were treated with biotinylated goat anti-rabbit IgG or anti-mouse IgG and a streptavidin-peroxidase complex (1:200; Vector, Burlingame, CA, USA) for 2 h at 25 °C. Sections were visualized by reaction with 3,3′-diaminobenzidine tetrachloride (Sigma) in 0.1 M Tris-HCl buffer (pH 7.2) and mounted on gelatin-coated slides. Sections were dehydrated and mounted in Canada balsam (Kanto, Tokyo, Japan).

Counting of NeuN immunoreactive neurons at the center of the hippocampal CA1 region was performed using an analysis system equipped with a computer-based CCD camera (OPTIMAS software version 6.5; CyberMetrics® Corporation, Phoenix, AZ, USA; magnification, × 100). The image was converted to a gray-scale image and NeuN immunoreactive neurons were automatically selected according to the intensity of NeuN immunohistochemical staining. Cell counts were averaged from 5 sections at 90-μm intervals from each gerbil. Values are demonstrated as a percentage of that obtained from the control group.

2.11. Measurement of lipid peroxidation and nitric oxide levels in the hippocampal homogenates

The levels of 4-hydroxy-2-nonenal (HNE) and nitric oxide (NO) were assessed to determine the protective mechanisms of Tat-PDIA3 against ischemic damage. Animals in the sham-operated and Tat peptide-, control-PDIA3-, and Tat-PDIA3-treated groups ($n = 15$ in each group) were anesthetized with 1.5 g/kg urethane at 3, 12, and 24 h after ischemia/reperfusion ($n = 5$ at each time point). The hippocampi were dissected out, and HNE was measured using a Bioxytech HAE-586 spectrophotometric assay kit (OxisResearch, Portland, OR, USA). We indirectly measured NO by quantifying nitrite, a stable oxidation product of NO, using Griess' method (Guevara et al., 1998). Hippocampi were homogenized in a buffer containing 10 mM 4-(2-hydroxyethyl)-1-piperazineethanesulfonic acid (pH 7.5), 200 mM mannitol, 70 mM sucrose, 1 mM ethylene glycol tetraacetic acid, and 5 mM butylated hydroxytoluene. We extracted 1 mL of homogenate with dichloromethane, and an aliquot of the lower organic phase was dried under nitrogen and reconstituted with water. The sample was mixed with *N*-methyl-2-phenylindole in acetonitrile and methanesulfonic acid before being incubated and centrifuged (3000 × *g* at 4 °C for 10 min). The absorbance of the clear supernatant was determined at 586 nm using a Beckman DU-64 spectrophotometer (Beckman, Fullerton, CA, USA). The HNE concentrations in the experimental samples were determined against HNE standards provided in the assay kit.

2.12. Quantitative PCR

The levels of BiP and CHOP were assessed to observe the ER stress-mediated activity of Tat-PDIA3 against ischemic damage. Animals in the sham-operated and Tat peptide-, control-PDIA3-, and Tat-PDIA3-treated groups ($n = 10$ in each group) were anesthetized with 1.5 g/kg urethane at 12 h and 4 days after ischemia/reperfusion ($n = 5$ at each time point), and the hippocampi were dissected out from the brain. We performed RNA extraction using a total RNA isolation kit (Macherney-Nagel, Düren, Germany). Spectrophotometric measurements were conducted using the Nanodrop Spectrophotometer (Nanodrop Technologies, Wilmington, DE, USA) to determine the RNA concentration and purity. We synthesized cDNA using 50 U of SuperScript II reverse transcriptase (Thermo Fisher Scientific, Carlsbad, CA, USA). Quantitative real-time PCR was performed as described by Cai et al. (2014). The primers used for real-time quantitative PCR were as follows: 5′-GCGGATCAAGGTGAAGAAA-3′ (forward) and 5′-TCCTGACCA GCCACGAAC-3′ (reverse) for BiP, 5′-GCCTTTCGCCTTTGAGACAGT-3′ (forward) and 5′-TGAGATATAGGTGCCCCCAATT-3′ (reverse) for CHOP, and 5′-CACACTGTGCCCATCTATGA-3′ (forward) and 5′-CCAT CTCTTGCTCGAAGTCT-3′ (reverse) for β-actin. Briefly, amplification was performed using an initial 10-min step at 95 °C, followed by 50 cycles for 15 s at 95 °C, 5 s at 60 °C, and 4–12 s at 72 °C, and a final extension for 10 min at 72 °C. Specificity of the product was confirmed with a melting-curve analysis. Quantification was performed using reaction kinetics data, and expression levels were related to β-actin.

2.13. Statistical analysis

The data were expressed as the mean of the experiments performed for each experimental investigation. In order to determine the effectiveness of Tat-PDIA3 against ischemic damage, mean differences among the groups were analyzed statistically by one-way or two-way analyses of variance followed by Bonferroni's post-hoc test using GraphPad Prism 5.01 software (GraphPad Software, Inc., La Jolla, CA, USA). All biochemical assays were conducted in triplicate. Biochemical assays were conducted in triplicates. The results were considered to be statistically significant if $p < 0.05$.

3. Results

3.1. Expression and purification of the Tat-PDIA3 protein

The human *PDIA3* gene fused to a Tat peptide expression vector to produce the Tat-PDIA3 fusion protein. The control-PDIA3 protein was manufactured without a Tat domain (Fig. 1A). The Tat-PDIA3 fusion protein was purified following overexpression using a Ni^{b+}- → Ni^{2+}-nitrilotriacetic acid Sepharose affinity column and PD-10 column chromatography. Using SDS-PAGE and western blot analyses, we confirmed the separation of purified proteins. The use of 15% SDS-PAGE and rabbit anti-polyhistidine antibody produced prominent bands on the western blot (Fig. 1A).

3.2. Transduction of the Tat-PDIA3 protein into HT22 and PDIA3 knockout cells

We treated HT22 and PDIA3 knockout cells with different concentrations (0.5–3 μM) of Tat-PDIA3 protein for various durations (15–60 min) to observe the *in vitro* efficacy of transducing Tat-PDIA3 protein into hippocampal cells. The Tat-PDIA3 fusion protein was transduced efficiently into HT22 and PDIA3 knockout cells, in a dose-dependent manner, by the 60-min time point (Fig. 1B). In addition, treatment with 3 μM Tat-PDIA3 significantly increased the time-dependent transduction of the protein into HT22 and PDIA3 knockout cells by 60 min after treatment (Fig. 1C). Following Tat-PDIA3 treatment, the expression of PDIA3 protein was found in lower

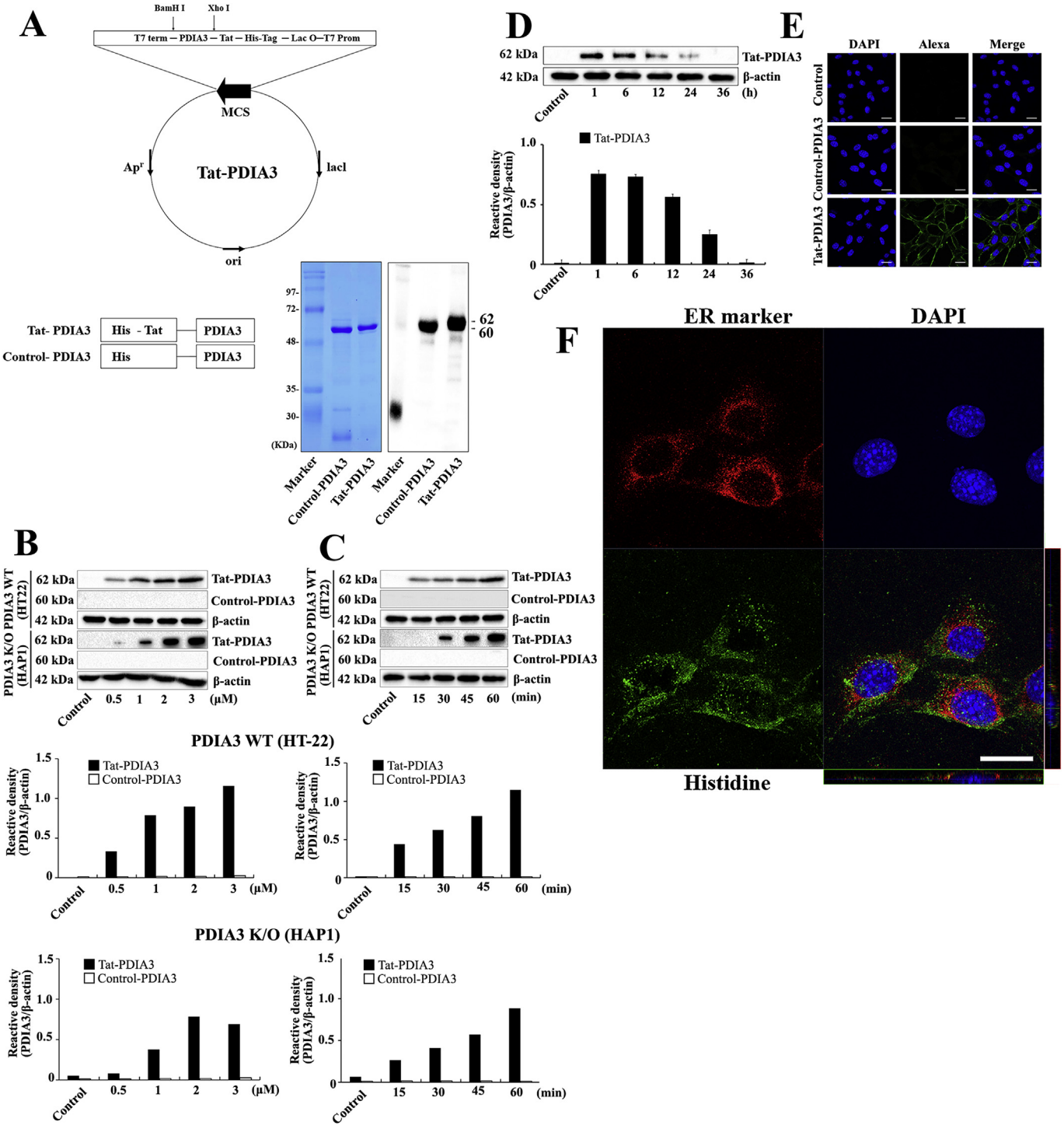

Fig. 1. Purification and transduction of the Tat-PDIA3 protein into HT22 hippocampal cells and/or PDIA3-knockout (KO) HAP1 cells. (A) Overview of the Tat-PDIA3 protein. Expression and purification of the Tat-PDIA3 protein and control-PDIA3 protein, as assessed by western blot analyses using the anti-histidine antibody. (B) Dose-dependent (0.5–3 μM) expression of PDIA3 1 h after Tat-PDIA3 treatment. (C) The time-dependent (0–60 min) expression of PDIA3, analyzed after treatment with 3 μM control-PDIA3 or Tat-PDIA3. (D) Time-dependent changes (1–36 h) in PDIA3 expression after control-PDIA3 or Tat-PDIA3 protein transduction for 1 h. (E) Localization and (F) co-localization of transduced Tat-PDIA3 protein observed with histidine and/or KDEL ER marker immunocytochemical staining in HT22 cells using confocal fluorescence microscopy. Images of orthogonal view are also shown to confirm the colocalization of Tat-PDIA3 protein with ER marker. Scale bar = 20 μm. The bars indicate the mean ± the standard error of the mean.

concentrations and at earlier time points in HT22 cells than in PDIA3 knockout cells, respectively (Fig. 1B and C). However, treatment with control-PDIA3 did not show transduction of PDIA3, at any time or dose exposure, in the HT22 and PDIA3 knockout cells (Fig. 1B and C).

The stability of transduced Tat-PDIA3 after treatment varied in the HT22 cells. Intracellular PDIA3 expression was significantly increased 0.5 h after Tat-PDIA3 treatment, but decreased thereafter in a time-dependent manner. Although prominent intracellular levels of transduced Tat-PDIA3 were still detected 24 h after treatment in HT22 cells, the expression was barely detectable at 36 h after treatment (Fig. 1D).

Cells were stained with histidine and DAPI to observe the intracellular distribution of the transduced Tat-PDIA3 protein in the

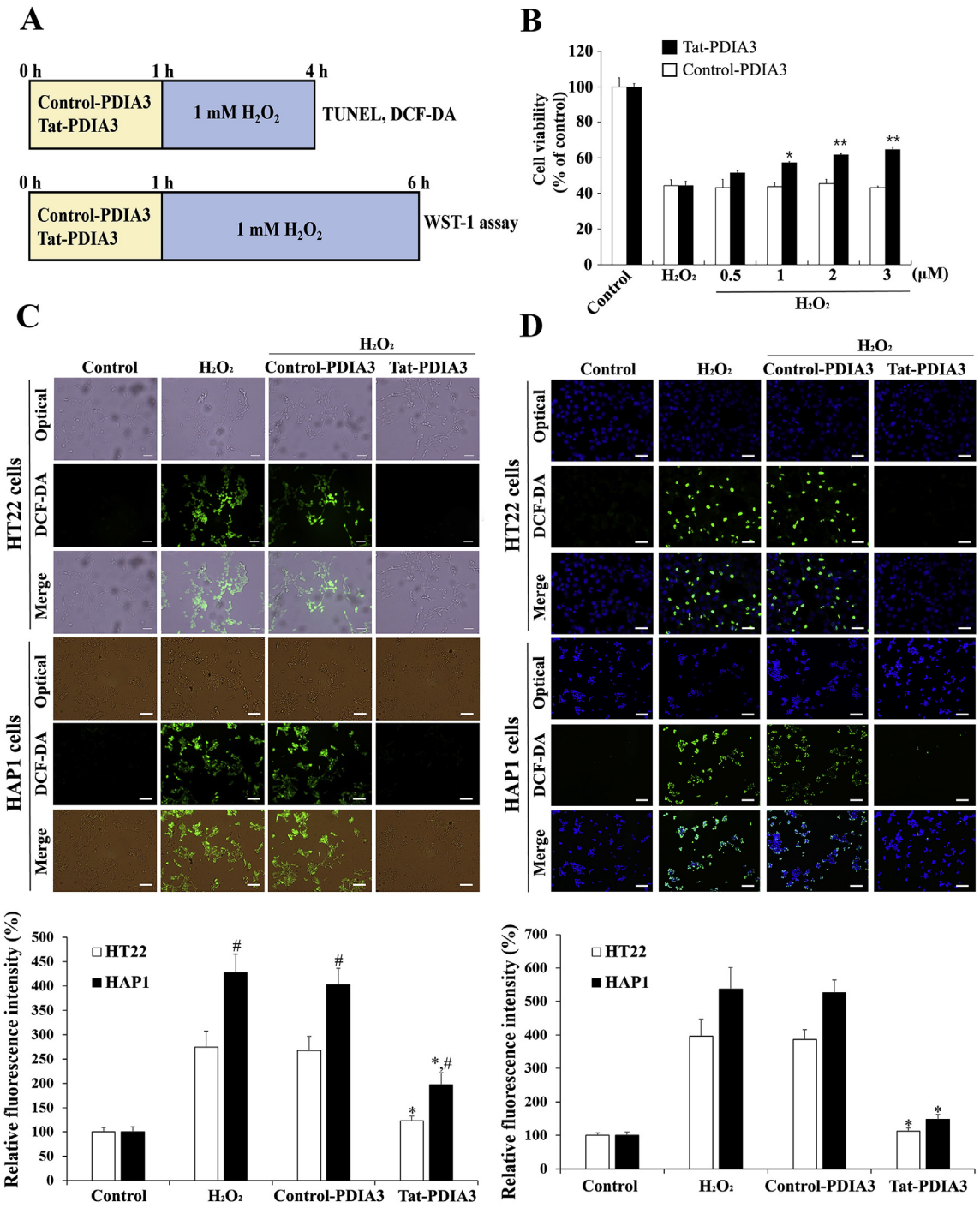

Fig. 2. Protective effects of transduced Tat-PDIA3 protein on ROS damage following exposure to 1 mM H_2O_2 in HT22 and PDIA3 knockout (KO) HAP1 cells. (A) Schematic drawing of the experimental design. (B) Dose-dependent (0.5–3 μM) effects of control-PDIA3 or Tat-PDIA3 on H_2O_2-induced cell damage in HT22 hippocampal cells, analyzed by the WST-1 assay. (C) ROS production was determined by measuring the DCF-DA fluorescence intensity in HT22 and PDIA3 KO HAP1 cells using an ELISA plate reader. (D) DNA fragmentation was assessed by TUNEL staining HT22 and PDIA3 KO HAP1 cells. Scale bar = 50 μm (C and D). Data were analyzed by two-way analyses of variance followed by Bonferroni's post-hoc tests. $^{*}p < 0.05$ and $^{\#}p < 0.05$ vs. the H_2O_2-treated group and HT22 group, respectively. The bars indicate the mean ± the standard error of the mean.

HT22 hippocampal cells. The cytoplasm and cell membrane were immunopositive for histidine 1 h after Tat-PDIA3 treatment, while histidine immunoreactivity was not detectable in the control group or in the cells treated with Control-PDIA3 (Fig. 1E).

We confirmed the localization of transduced Tat-PDIA3 proteins in the HT22 hippocampal cells by double immunocytochemical staining for PDIA3 and the KDEL ER marker at 24 h after treatment. This experiment revealed the presence of some PDIA3-immunoreactive structures in the ER of HT22 cells, although some PDIA3 immunoreactivity was also detected in the membrane or cytoplasm (Fig. 1F).

3.3. Neuroprotective effects of transduced Tat-PDIA3 on H_2O_2-induced oxidative damage

The neuroprotective effects of transduced Tat-PDIA3 on HT22 cells

with H_2O_2-induced oxidative damage were assessed by a WST-1 assay for cell viability, as shown in Fig. 2A. Exposure to 1 mM H_2O_2 caused prominent cell death, with only 43.4–45.6% of HT22 cells remaining in the control group. Treatment using Tat-PDIA3 significantly and dose-dependently reduced the cell death of HT22 cells exposed to H_2O_2. Following treatment with 3 μM Tat-PDIA3 after 5 h of exposure to 1 mM H_2O_2, 64.8% of the HT22 cells remained (Fig. 2B).

The presence of DCF-DA-positive and TUNEL-positive cells confirmed the formation of ROS in HT22 and PDIA3 knockout cells with H_2O_2-induced oxidative damage. Treatment with H_2O_2 significantly elevated DCF-DA and TUNEL fluorescence in HT22 and HAP1 cells compared to those in control group, respectively (Fig. 2C and D). Notably, the DCF-DA fluorescence was significantly higher in PDIA3 knockout cells than in HT22 cells (Fig. 2C). Treatment with control-PDIA3 protein did not induce any prominent changes in cell viability, ROS formation, or TUNEL fluorescence in HT22 and PDIA3 knockout cells exposed to H_2O_2. In contrast, treatment with Tat-PDIA3 significantly reduced the DCF-DA and TUNEL fluorescence in both HT22 and PDIA3 knockout cells compared to those in H_2O_2 alone group, although some DCF-DA and TUNEL fluorescence was present in PDIA3 knockout cells (Fig. 2C and D). In HT22 and PDIA3 knockout cells, administration of Tat-PDIA3 reduced TUNEL fluorescence compared to that in the H_2O_2 alone or Control-PDIA3-treated group and the difference in TUNEL fluorescence was similarly detected between HT22 and PDIA3 knockout cells (Fig. 2C and D).

3.4. Neuroprotective effects of Tat-PDIA3 against ischemic damage in the gerbil hippocampus

In the sham-operated group, animals did not show any significant changes in locomotor activity either 1 day before or 1 day after the sham operation (Fig. 3A). Moreover, NeuN-immunoreactive neurons were abundant in all regions of the hippocampus, including the hippocampal CA1 region 4 days after the sham operation (Fig. 3B). In the Tat peptide-treated group, locomotor activity was significantly enhanced 1 day after ischemia/reperfusion compared to that in the sham-operated group, and the average ratio of locomotor activity 1 day before ischemia/reperfusion to that 1 day after was 2.91. In this group, NeuN-immunoreactive neurons were abundant in the hippocampal CA2/3 region, while a few neurons were observed in the hippocampal CA1 region 4 days after ischemia/reperfusion. In the control-PDIA3-treated group, locomotor activity was significantly elevated 1 day after ischemia/reperfusion compared to that in the sham-operated group, and the ratio of locomotor activity was similar to that of the Tat peptide-treated group. The number of NeuN-immunoreactive neurons in the hippocampal CA1 region of the control-PDIA3-treated group was significantly reduced compared to that in the sham-operated group 4 days after ischemia/reperfusion; however, it was similar to that of the Tat peptide-treated group. In the Tat-PDIA3-treated group, locomotor activity was significantly enhanced 1 day after ischemia/reperfusion compared to that in the sham-operated group. However, the locomotor activity ratio of the Tat-PDIA3-treated group was significantly lower than that of the Tat peptide-treated group (Fig. 3A). In Tat-PDIA3-treated group, there were many NeuN-immunoreactive neurons, i.e., 51.2% of the hippocampal CA1 neurons were NeuN positive compared to that in the sham-operated group (Fig. 3B).

3.5. Effects of Tat-PDIA3 on ischemia-induced glial activation in the hippocampal CA1 region

In the sham-operated group, GFAP-immunoreactive astrocytes had small cytoplasm with thin processes and Iba-1-immunoreactive microglia had a small, round cytoplasm with long, thin processes 4 days after the operation. In the Tat peptide-treated group, GFAP-immunoreactive astrocytes exhibited hypertrophic cytoplasm with a punctuate morphology and Iba-1-immunoreactive microglia had hypertrophic cytoplasm with retracted processes 4 days after ischemia/reperfusion. In addition, the Iba-1-immunoreactive microglia, which are found following neuronal death, were abundant in the stratum pyramidale of the Tat peptide-treated group. In the control-PDIA3-treated group, the distribution and morphology of GFAP-immunoreactive astrocytes and Iba-1-immunoreactive microglia were similar to those in the Tat peptide-treated group 4 days after ischemia/reperfusion. In the Tat-PDIA3-treated group, some GFAP-immunoreactive astrocytes and Iba-1-immunoreactive microglia showed hypertrophic cytoplasm with retracted processes (Fig. 4).

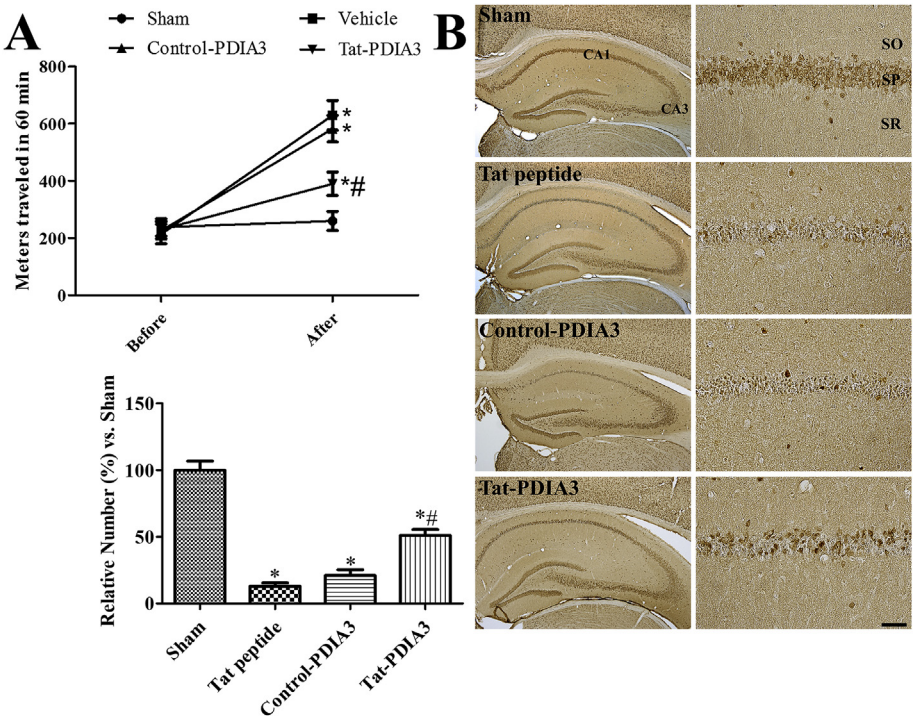

Fig. 3. Protective effects of Tat-PDIA3 protein against ischemic damage in gerbils. (A) The locomotor activity in gerbils 1 day before and after ischemia/reperfusion in the sham-operated group and the Tat peptide-, control-PDIA3-, and Tat-PDIA3-treated ischemic groups. Spontaneous locomotor activity was evaluated in terms of the entire distance (meters) traveled for 60 min before and 1 d after ischemia/reperfusion ($n = 5$ per group; $^{*}p < 0.05$ vs. from the same group measured before surgery, $^{\#}p < 0.05$ vs. the Tat peptide-treated group). The bars indicate the standard error of the mean. (B) Immunohistochemistry for NeuN in the hippocampus and magnified CA1 region of the sham-operated group and the Tat peptide-, control-PDIA3-, and Tat-PDIA3-treated ischemic groups 4 d after ischemia/reperfusion. The number of NeuN-immunoreactive neurons in each group relative to that in the sham-operated group, per section, is shown ($n = 5$ per group; $^{*}p < 0.05$ vs. the sham-operated group, $^{\#}p < 0.05$ vs. the Tat peptide-treated group). The bars indicate the standard error of the mean. Scale bar = 350 μm (whole hippocampus) and 50 μm (CA1 region).

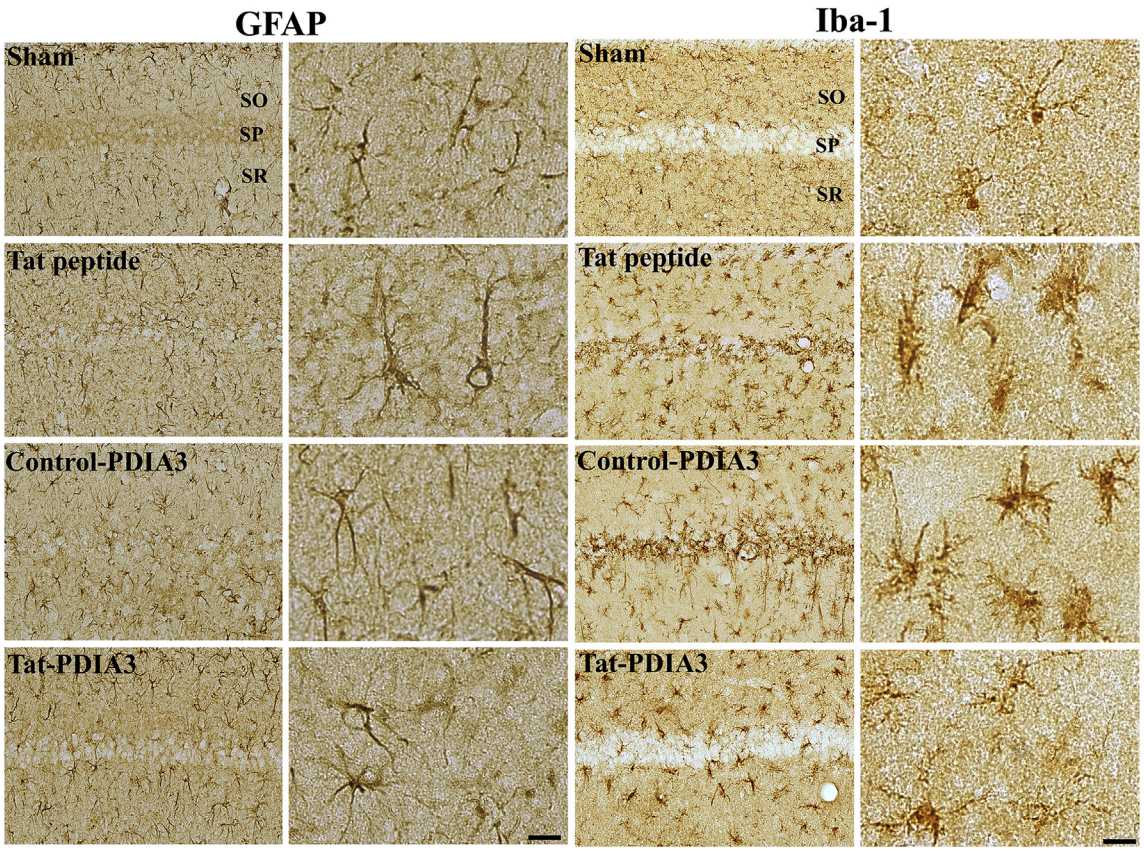

Fig. 4. Immunohistochemistry for GFAP and Iba-1 in the CA1 region of the sham-operated group and the Tat peptide-, control-PDIA3-, and Tat-PDIA3-treated ischemic groups 4 d after ischemia/reperfusion. High magnified images are also shown to demonstrate the morphology of astrocytes and microglia. SP, stratum pyramidale; SO, stratum oriens; SR, stratum radiatum. Scale bar = 50 μm.

3.6. Effects of Tat-PDIA3 on ischemia-induced lipid peroxidation in the hippocampus

The HNE protein levels in the hippocampal homogenates did not significantly change at 3, 12, or 24 h after the sham operation among groups. However, the ischemia-operated groups showed significant changes in the hippocampal homogenate HNE levels at 3, 12, and 24 h after ischemia/reperfusion compared to time-matched sham operated group. The HNE level in all ischemia-operated groups was significantly higher than that in the sham-operated group 3 h after ischemia/reperfusion, after which the HNE protein levels decreased. However, the HNE level was significantly lower in the Tat-PDIA3-treated group than in the Tat peptide-treated or control-PDIA3-treated group by 24 h after ischemia/reperfusion. HNE level was similarly observed in the Tat-PDIA3 treated group compared to sham operated group 24 h after ischemia/reperfusion (Fig. 5A).

3.7. Effects of Tat-PDIA3 on NO generation in the hippocampus

Similar to the HNE levels, the NO levels in the hippocampal homogenates did not significantly change at 3, 12, or 24 h after the sham operation. However, the NO levels were significantly elevated 3 h after ischemia/reperfusion and were further elevated 12 and 24 h after ischemia/reperfusion in the Tat peptide-treated and control-PDIA3-treated groups when compared to the sham-operated group. The NO levels were significantly lower at 3 and 24 h after ischemia/reperfusion in the Tat-PDIA3-treated group than in the Tat peptide-treated or control-PDIA3-treated group (Fig. 5B).

3.8. Effects of Tat-PDIA3 on ischemia-induced BiP and CHOP in the hippocampus

Sham-operated animals did not show any significant changes in UPR elements at 12 h or 4 days after the sham operation. In all ischemic groups, the BiP and CHOP mRNA levels were significantly elevated at 12 h and 4 days after ischemia/reperfusion compared to those in the time-matched sham-operated animals. The BiP mRNA levels were higher in the Tat-PDIA3-treated group than in the Tat peptide- or control-PDIA3-treated group at 12 h and 4 days after ischemia/reperfusion, although the differences were not statistically significant. In contrast, the CHOP mRNA levels were significantly higher in the Tat peptide- or control-PDIA3-treated group than in the Tat-PDIA3-treated group at 12 h and 4 days after ischemia/reperfusion (Fig. 5C).

4. Discussion

Prior research has shown that PDIA3, a multifunctional protein that is located mostly at the ER lumen, participates in the folding of numerous cysteine-rich glycoproteins (Ellgaard and Frickel, 2003). In addition, PDIA3 functions as a molecular chaperone that prevents the formation of protein aggregates during ER stress by facilitating the function of disulfide isomerase in nascent and denatured proteins with a thioredoxine-like domain (Ferrari and Söling, 1999; Grubb et al., 2012; Hatahet and Ruddock, 2009; Kozlov et al., 2010; Määttänen et al., 2010). However, PDI is known to be susceptible to oxidative damage, as outlined by the effects of lipid aldehyde (Carbone et al., 2005) and the significant inhibition of its thiol reductase activity in neurons 24 h after hypoxia (Liu et al., 2015). As such, the goal of this study was to test the hypothesis that the administration of Tat-PDIA3 would protect hippocampal neurons from ischemic damage. Further, to

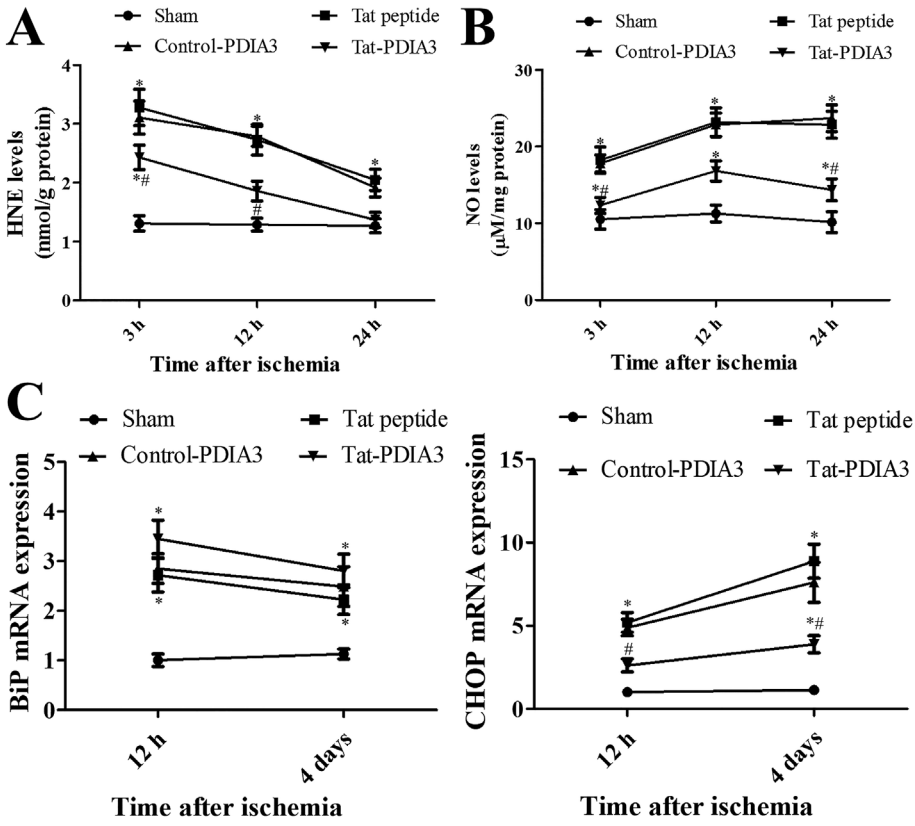

Fig. 5. Effects of Tat-PDIA3 protein on lipid peroxidation and NO production, as well as on the BiP and CHOP mRNA levels, in the gerbil hippocampus. Analysis of (A) HNE, (B) NO, and (C) BiP and CHOP mRNA levels in the hippocampal homogenates in the sham-operated group and the Tat peptide-, control-PDIA3-, and Tat-PDIA3-treated ischemic groups ($n = 5$ per time point, $^{*}p < 0.05$ vs. the sham-operated group, $^{\#}p < 0.05$ vs. the Tat peptide-treated group. Bars indicate the mean ± the standard error of the mean.

confirm the effects of Tat-PDIA3 against oxidative stress, we also used PDIA3 knockout cells.

To achieve our objective, we first generated a Tat-PDIA3 fusion protein to facilitate the cell penetration of PDIA3 into HT22 hippocampal neurons and PDIA3 knockout cells. The transduction of Tat-PDIA3 into HT22 hippocampal cells and PDIA3 knockout cells was efficient, dose-dependent, and stable by 24 h after treatment in HT22 cells. This result is consistent with our previous study, in which Tat-nucleolar protein 3 fusion protein can be detectable in HT22 cells by 60 h after treatment (Sohn et al., 2016). The transduced PDIA3 proteins were localized in the cell surface and cytoplasm of the HT22 hippocampal cells, and we confirmed that some transduced Tat-PDIA3 immunoreactivity was present in the ER of cells in the hippocampal CA1 region. The results of previous studies showing that PDIA3 is distributed over the surface and perinuclear area of the ER in MC3T3-E1 osteoblasts and motoneuron-like neural stem cells (Chen et al., 2013a; Yoo et al., 2017) support our results. Thus, our findings suggest that the Tat-PDIA3 fusion protein was efficiently transduced into the cytoplasm and ER, without cell-surface binding.

It is known that ROS cause neuronal damage by interacting with the cell membrane and DNA. In the present study, we found that Tat-PDIA3 exhibited neuroprotective effects against H_2O_2-induced oxidative damage in HT22 hippocampal cells and PDIA3 knockout cells. Herein, we measured cell death using TUNEL staining at 3 h after H_2O_2 exposure and measured proliferating cells at 5 h after H_2O_2 exposure with WST-1 assays to confirm the roles of Tat-PDIA3 against neuronal damage in HT22 and PDIA3 knockout cells. In HT22 cells, exposure to 1 mM H_2O_2 significantly reduced cell viability, with about half of the cells exhibiting signs of neuronal death stained with TUNEL. However, pre-incubation with Tat-PDIA3 significantly enhanced the HT22 cell viability after H_2O_2 exposure. In parallel with this result, ROS formation and DNA fragmentation, which were measured using DCF-DA and TUNEL staining, respectively, were significantly reduced in Tat-PDIA3-treated HT22 cells after exposure to H_2O_2. This result is consistent with that of a previous study showing that the overexpression of PDI protects neurons exposed to anoxia (Liu et al., 2015). In addition, the overexpression of PDI with cyclopentenone prostaglandins decreases cell death via the inactivation of proapoptotic proteins, such as caspases 3 and 9, and the attenuation of ER stress (Liu et al., 2015). As for PDIA3 knockout cells, exposure to 1 mM H_2O_2 induced ROS generation and cell death that was more severe than that in HT22 cells; however, treatment with Tat-PDIA3 protected against the H_2O_2-induced ROS generation and TUNEL fluorescence in PDIA3 knockout cells. This result suggests that constitutively expressed PDIA3 may reduce the neuronal damage induced by oxidative stress, while the supplementation of Tat-PDIA3 further lowers the oxidative stress and cell damage. This result is supported by a previous study demonstrating that ablation of PDIA3 causes accelerated cell death in liver cells (Yuan et al., 2017a) and chondrocytes (Linz et al., 2015). Moreover, the ablation of PDIA3 exhibited increased ROS levels in the liver during aging (Yuan et al., 2017a).

In the present study, we also measured the neuroprotective effects of Tat-PDIA3 against ischemic damage in the hippocampal neurons of Mongolian gerbils, which are widely used as an animal model for ischemia (Ginsberg and Busto, 1989). Given its incomplete circle of Willis (Du et al., 2011), these animals lack the posterior communicating arteries between the carotid and vertebral arteries. Since ischemic damage can lead to hyperactivity 1 day after ischemia/reperfusion, we observed locomotor activity at this time point, although we could not observe any neuronal death in this time point (Andersen et al., 1997; Suzuki et al., 1983). In the present study, Tat peptide-treated animals showed significantly enhanced locomotor activity 1 day after ischemia/reperfusion compared to sham-operated group. The control-PDIA3-treated group showed a similar result, although locomotor activity in this group was slightly reduced compared to that in the vehicle-treated group. The administration of Tat-PDIA3 significantly ameliorated the ischemia-induced hyperactivity 1 day after ischemia/reperfusion. Consistent with the locomotor activity, morphological evidence based on NeuN immunohistochemistry showed that the administration of Tat-PDIA3, but not Tat peptide or Control-PDIA3, significantly increased

the number of NeuN-immunoreactive neurons in the hippocampal CA1 region 4 days after ischemia/reperfusion. Several studies in a variety of models have shown that PDI is protective and helps reduce damage. For example, the overexpression of PDI significantly reduced the number of TUNEL-positive CA1 neurons after transient forebrain ischemia (Truettner et al., 2009); however, that study failed to observe PDI mRNA changes in the hippocampus. In addition, PDI ameliorates the reduction in the apoptotic rate and prevents cardiac remodeling in human infarcted hearts (Severino et al., 2007). In our previous study, we found reduced PDIA3 protein levels 3 h after spinal cord ischemia and demonstrated that Tat-PDIA3 treatment significantly ameliorated the spinal cord ischemia-induced behavioral and morphological changes in rabbits (Yoo et al., 2017). Despite these known beneficial effects, other studies have demonstrated that PDI can also exert detrimental effects. In a neurodegenerative model, the inhibition of PDI reduced the toxicity of mutant huntingtin exon 1 and amyloid beta peptides processed from amyloid precursor protein (Hoffstrom et al., 2010). In murine embryonic fibroblast cells, the inhibition of PDIA3 by short hairpin RNA significantly decreases cell death and caspase-3/7 activation by actinomycin D or tunicamycin (Zhao et al., 2015a). Conversely, the overexpression of PDIA3 significantly increases cell death and caspase-3/7 activation (Zhao et al., 2015a). Another study showed that PDIA3 expression protects against methamphetamine-induced cell toxicity, at least in neuroblastoma cell lines (Pendyala et al., 2012). Likewise, in the prion-related model, PDI expression protects cells against the scrapie isoform of prion protein toxicity (Hetz et al., 2005). The discrepancy between beneficial and detrimental effects of PDI may be associated with the *S*-nitrosylation of PDI by NO. That is, while PDI itself attenuates the neuronal cell death that is caused by ER stress, misfolded proteins, or proteasome inhibition, the *S*-Nitrosylation of PDI by NO prevents PDI from exerting its neuroprotective effects against various models of cell damage (Uehara et al., 2006). A recent study demonstrated that PDI acts as an anti-apoptotic factor in initial ER stress, but constant ER stress promotes the apoptosis by releasing PDIA3 from the ER lumen to induce Bak-dependent mitochondrial outer membrane permeabilization in PC12 cells exposed to tetrachlorobenzoquinone (Liu et al., 2017).

Here, we also observed that the administration of Tat-PDIA3, but not Tat peptide or control-PDIA, significantly reduced ischemia-induced astrocyte and microglial activation, known as reactive gliosis (Pekny et al., 2014). The activation of astrocytes and microglia, which is induced by ischemia, increases GFAP expression through hypertrophic morphology and cell proliferation, and subsequently facilitates the secretion of cytokines. Similarly, activated microglia increase the expression of major histocompatibility complex antigens and costimulatory molecules (Finsen et al., 1993; Zhang et al., 2002), as well as the synthesis of neuro-inflammatory mediators (Ceulemans et al., 2010). In the current study, given the better morphological and functional outcomes following ischemic damage in the Tat-PDIA3-treated group vs. the Tat-peptide- or control-PDIA3-treated group, the reduction of astrocyte and microglia activation may be the mechanism underlying the neuroprotective effects of Tat-PDIA3 against ischemic damage in the hippocampal CA1 region (Barreto et al., 2011; Tikka et al., 2001).

Prior research has demonstrated that ER stress-induced accumulation of unfolded or misfolded proteins increases BiP dissociation (Lee et al., 2010), which serves as a marker for ER stress. Moreover, the accumulation of unfolded and misfolded proteins causes ROS production (Enyedi et al., 2010; Merksamer et al., 2008), ultimately leading to neuronal damage in the brain (Malhotra and Kaufman, 2007). Interestingly, oxidative stress also directly alters the activity of PDIs in many human diseases (Nakamura and Lipton, 2011). In the present study, our DCF-DA analysis revealed that treatment with Tat-PDIA3 significantly reduced the H_2O_2-induced ROS formation. Additionally, the administration of Tat-PDIA3 significantly reduced the ischemia-induced lipid peroxidation, a reliable indicator of neuronal damage (Bromont et al., 1989), in the gerbil hippocampus (McKracken et al., 2004; Wang et al., 2006). This result is consistent with that of previous studies, wherein PDIA3 expression reduced methamphetamine-induced intracellular ROS production in a neuroblastoma cell line (Pendyala et al., 2012). Genetic ablation of PDIA3 upregulates the UPR in the cartilage (Linz et al., 2015) and liver (Yuan et al., 2017a), with sustained phosphorylation of protein kinase R-like endoplasmic reticulum kinase and eukaryotic initiation factor1α.

Our study additionally demonstrated ER stress-induced activation of the UPR in hippocampal homogenates by real-time quantitative PCR, likely because the UPR can re-establish homeostasis or facilitate the apoptotic process in cells. The BiP and CHOP mRNA levels were also significantly increased after transient forebrain ischemia. This result was consistent with previous studies showing that BiP expression is increased in the damaged brain areas in both focal and global ischemic models (Ito et al., 2001; Oida et al., 2008; Roberts et al., 2007; Shibata et al., 2003; Tajiri et al., 2004). In the present study, the administration of Tat-PDIA3 elevated the BiP mRNA levels in the hippocampus at 12 h and 4 days after ischemia relative to those in the Tat peptide- or control-PDIA3-treated group. Several lines of evidence demonstrate that BiP expression protects neurons from the damage that is induced by ER stress (Rao et al., 2002; Schröder and Kaufman, 2005). In addition, treatment with BiP inducer X significantly increases BiP mRNA in the hippocampus and protects neurons from ischemic cell death in the gerbil hippocampus after transient forebrain ischemia (Oida et al., 2008); BiP also protects the mouse cerebral cortex from focal cerebral ischemia-induced damage (Kudo et al., 2008). In contrast, the degradation of BiP mRNA facilitates neuronal cell death via calcium release from the ER (Gomer et al., 1991). ER stress induced by cardiac arrest is diminished after hydrogen-rich saline treatment by upregulating BiP expression from 6 h to 24 h after return of spontaneous circulation and by downregulating CHOP expression in the hippocampus (Gao et al., 2017).

In the present study, CHOP mRNA levels were significantly reduced in the Tat-PDIA3-treated group compared to the levels in the Tat peptide- or control-PDIA3-treated group. Given that TUNEL-positive cells were found to be co-localized with CHOP-positive cells in the hippocampus of diabetic mice (Zhao et al., 2015b) and in the hippocampal CA1 region of ischemic gerbils (Oida et al., 2008), these suggest that CHOP participates in the control of neuronal death in the hippocampus (Liu et al., 2013; Oyadomari and Mori., 2004; Paz Gavilán et al., 2006; Tajiri et al., 2004). In contrast, CHOP small interfering RNA treatment significantly reduces Bim-caspase 3 apoptotic pathway activity, increases anti-apoptotic B-cell lymphoma 2 pathway activity, and finally ameliorates the brain injury that is induced by subarachnoid hemorrhage (He et al., 2012). CHOP deficient mice showed reduction in cleavage of procaspase-3 and the induction of Bax protein in the kidney after ischemia/reperfusion compared to that in the control mice (Noh et al., 2015). Finally, the present study identified that NO contributes to neuronal cell injury, in part by triggering the accumulation of misfolded proteins through the *S*-nitrosylation of PDI by NO, which forms SNO-PDI (Nakamura and Lipton., 2009; Uehara et al., 2006). We found that the NO level was significantly elevated, in a time-dependent manner, in the hippocampal homogenates 24 h after ischemia/reperfusion. However, the administration of Tat-PDIA3 significantly ameliorated the ischemia-induced NO levels in the hippocampal homogenates. Nonetheless, we could not determine whether PDIA3 directly reduced the NO level or if the NO level was depleted by the formation of SNO-PDI; thus, further studies addressing this issue are needed.

In summary, our results show that Tat-PDIA3 underwent efficient transduction *in vitro* and *in vivo* and significantly attenuated the H_2O_2-induced neuronal damage by reducing the oxidative stress in hippocampal cells. We also demonstrated that ablation of PDIA3 exacerbates the H_2O_2-induced oxidative stress and cell damage. To the best of our knowledge, the present study is the first trials to show roles of PDIA3 proteins, not RNAs or DNAs, against ischemic damage likely by attenuating the oxidative damage and ER response-induced apoptosis

through CHOP.

Conflicts of interest

All authors have approved the manuscript for submission, and we have no conflicts of interest to disclose.

Authors' contributions

DYY, SBC, HYJ, WK, KYL, SMM, MHW, JHC, DWK, SYC, and IKH conceived of the study. DYY, SBC, SYC, and IKH designed the study. DYY, HYJ, WK, KYL, JHC, and IKH conducted the animal experiments and SBC, DWK, and SYC conducted the biochemical experiments. SMM and MHW participated in designing and discussing the study. All authors have read and approved the final manuscript.

Data availability

The datasets generated during and/or analyzed during the current study are available from the corresponding author on reasonable request.

Acknowledgements

The authors would like to thank Dr. Seung-Hae Kwon of the Korean Basic Science Institute Chuncheon Center for the technical assistance with the confocal image analyses. This work was supported by the Basic Science Research Program through the National Research Foundation of Korea (NRF) funded by the Ministry of Education (NRF-2015R1D1A1A01059980 and 2015R1D1A3A01015668). In addition, this work was supported by the Promising-Pioneering Researcher Program through Seoul National University (SNU) in 2015 and by the Research Institute for Veterinary Science, Seoul National University.

Appendix A. Supplementary data

Supplementary data to this article can be found online at https://doi.org/10.1016/j.neuint.2018.11.002.

References

Andersen, M.B., Zimmer, J., Sams-Dodd, F., 1997. Postischemic hyperactivity in the Mongolian gerbil correlates with loss of hippocampal neurons. Behav. Neurosci. 111, 1205–1216.
Barreto, G., White, R.E., Ouyang, Y., Xu, L., Giffard, R.G., 2011. Astrocytes: targets for neuroprotection in stroke. Cent. Nerv. Syst. Agents Med. Chem. 11, 164–173.
Bradford, M.M., 1976. A rapid and sensitive method for the quantitation of microgram quantities of protein utilizing the principle of protein-dye binding. Anal. Biochem. 72, 248–254.
Bromont, C., Marie, C., Bralet, J., 1989. Increased lipid peroxidation in vulnerable brain regions after transient forebrain ischemia in rats. Stroke 20, 918–924.
Cai, X.H., Li, X.C., Jin, S.W., Liang, D.S., Wen, Z.W., Cao, H.C., Mei, H.F., Wu, Y., Lin, Z.D., Wang, L.X., 2014. Endoplasmic reticulum stress plays critical role in brain damage after chronic intermittent hypoxia in growing rats. Exp. Neurol. 257, 148–156.
Carbone, D.L., Doorn, J.A., Kiebler, Z., Petersen, D.R., 2005. Cysteine modification by lipid peroxidation products inhibits protein disulfide isomerase. Chem. Res. Toxicol. 18, 1324–1331.
Carette, J.E., Raaben, M., Wong, A.C., Herbert, A.S., Obernosterer, G., Mulherkar, N., Kuehne, A.I., Kranzusch, P.J., Griffin, A.M., Ruthel, G., Dal Cin, P., Dye, J.M., Whelan, S.P., Chandran, K., Brummelkamp, T.R., 2011. Ebola virus entry requires the cholesterol transporter Niemann-Pick C1. Nature 477, 340–343.
Castillo, V., Oñate, M., Woehlbier, U., Rozas, P., Andreu, C., Medinas, D., Valdés, P., Osorio, F., Mercado, G., Vidal, R.L., Kerr, B., Court, F.A., Hetz, C., 2015. Functional role of the disulfide isomerase ERp57 in axonal regeneration. PloS One 10, e0136620.
Ceulemans, A.G., Zgavc, T., Kooijman, R., Hachimi-Idrissi, S., Sarre, S., Michotte, Y., 2010. The dual role of the neuroinflammatory response after ischemic stroke: modulatory effects of hypothermia. J. Neuroinflammation 7, 74.
Chen, J., Doroudi, M., Cheung, J., Grozier, A.L., Schwartz, Z., Boyan, B.D., 2013a. Plasma membrane Pdia3 and VDR interact to elicit rapid responses to 1α,25(OH)$_2$D$_3$. Cell. Signal. 25, 2362–2373.
Chen, X., Sa'adedin, F., Deme, B., Rao, P., Bradshaw, J., 2013b. Insertion of TAT peptide and perturbation of negatively charged model phospholipid bilayer revealed by neutron diffraction. Biochim. Biophys. Acta 1828, 1982–1988.
Cominacini, L., Mozzini, C., Garbin, U., Pasini, A., Stranieri, C., Solani, E., Vallerio, P., Tinelli, I.A., Fratta Pasini, A., 2015. Endoplasmic reticulum stress and Nrf2 signaling in cardiovascular diseases. Free Radic. Biol. Med. 88, 233–242.
Doroudi, M., Chen, J., Boyan, B.D., Schwartz, Z., 2014. New insights on membrane mediated effects of 1α,25-dihydroxy vitamin D3 signaling in the musculoskeletal system. Steroids 81, 81–87.
Du, X.Y., Zhu, X.D., Dong, G., Lu, J., Wang, Y., Zeng, L., Zhao, T.Y., Ye, H.H., Li, R.S., Bai, J.Y., Chen, Z.W., 2011. Characteristics of circle of Willis variations in the Mongolian gerbil and a newly established ischemia-prone gerbil group. ILAR J. 52, E1–E7.
Ellgaard, L., Frickel, E.M., 2003. Calnexin, calreticulin, and ERp57: teammates in glycoprotein folding. Cell Biochem. Biophys. 39, 223–247.
Enyedi, B., Várnai, P., Geiszt, M., 2010. Redox state of the endoplasmic reticulum is controlled by *Ero*1L-alpha and intraluminal calcium. Antioxidants Redox Signal. 13, 721–729.
Eum, W.S., Kim, D.W., Hwang, I.K., Yoo, K.Y., Kang, T.C., Jang, S.H., Choi, H.S., Choi, S.H., Kim, Y.H., Kim, S.Y., Kwon, H.Y., Kang, J.H., Kwon, O.S., Cho, S.W., Lee, K.S., Park, J., Won, M.H., Choi, S.Y., 2004. In vivo protein transduction: biologically active intact pep-1-superoxide dismutase fusion protein efficiently protects against ischemic insult. Free Radic. Biol. Med. 37, 1656–1669.
Ferrari, D.M., Söling, H.D., 1999. The protein disulphide-isomerase family: unravelling a string of folds. Biochem. J. 339, 1–10.
Finsen, B.R., Jørgensen, M.B., Diemer, N.H., Zimmer, J., 1993. Microglial MHC antigen expression after ischemic and kainic acid lesions of the adult rat hippocampus. Glia 7, 41–49.
Gao, Y., Gui, Q., Jin, L., Yu, P., Wu, L., Cao, L., Wang, Q., Duan, M., 2017. Hydrogen-rich saline attenuates hippocampus endoplasmic reticulum stress after cardiac arrest in rats. Neurosci. Lett. 640, 29–36.
Ginsberg, M.D., Busto, R., 1989. Rodent models of cerebral ischemia. Stroke 20, 1627–1642.
Gomer, C.J., Ferrario, A., Rucker, N., Wong, S., Lee, A.S., 1991. Glucose regulated protein induction and cellular resistance to oxidative stress mediated by porphyrin photosensitization. Cancer Res. 51, 6574–6579.
Grubb, S., Guo, L., Fisher, E.A., Brodsky, J.L., 2012. Protein disulfide isomerases contribute differentially to the endoplasmic reticulum-associated degradation of apolipoprotein B and other substrates. Mol. Biol. Cell 23, 520–532.
Guevara, I., Iwanejko, J., Dembińska-Kieć, A., Pankiewicz, J., Wanat, A., Anna, P., Gołabek, I., Bartuś, S., Malczewska-Malec, M., Szczudlik, A., 1998. Determination of nitrite/nitrate in human biological material by the simple Griess reaction. Clin. Chim. Acta 274, 177–188.
Hatahet, F., Ruddock, L.W., 2009. Protein disulfide isomerase: a critical evaluation of its function in disulfide bond formation. Antioxidants Redox Signal. 11, 2807–2850.
He, Z., Ostrowski, R.P., Sun, X., Ma, Q., Tang, J., Zhang, J.H., 2012. Targeting C/EBP homologous protein with siRNA attenuates cerebral vasospasm after experimental subarachnoid hemorrhage. Exp. Neurol. 238, 218–224.
Hetz, C., Russelakis-Carneiro, M., Wälchli, S., Carboni, S., Vial-Knecht, E., Maundrell, K., Castilla, J., Soto, C., 2005. The disulfide isomerase Grp58 is a protective factor against prion neurotoxicity. J. Neurosci. 25, 2793–2802.
Hoffstrom, B.G., Kaplan, A., Letso, R., Schmid, R.S., Turmel, G.J., Lo, D.C., Stockwell, B.R., 2010. Inhibitors of protein disulfide isomerase suppress apoptosis induced by misfolded proteins. Nat. Chem. Biol. 6, 900–906.
Hwang, I.K., Yoo, K.Y., Kim, D.W., Han, B.H., Kang, T.C., Choi, S.Y., Kim, J.S., Won, M.H., 2005. Protein disulfide isomerase immunoreactivity and protein level changes in neurons and astrocytes in the gerbil hippocampal CA1 region following transient ischemia. Neurosci. Lett. 375, 117–122.
Ito, D., Tanaka, K., Suzuki, S., Dembo, T., Kosakai, A., Fukuuchi, Y., 2001. Up-regulation of the Ire1-mediated signaling molecule, Bip, in ischemic rat brain. Neuroreport 12, 4023–4028.
Jeong, H.J., Yoo, D.Y., Kim, D.W., Yeo, H.J., Cho, S.B., Hyeon, J., Park, J.H., Park, J., Eum, W.S., Hwang, H.S., Won, M.H., Hwang, I.K., Choi, S.Y., 2014. Neuroprotective effect of PEP-1-peroxiredoxin2 on CA1 regions in the hippocampus against ischemic insult. Biochim. Biophys. Acta 1840, 2321–2330.
Jung, H.Y., Cho, S.B., Kim, W., Yoo, D.Y., Won, M.H., Choi, G.M., Cho, T.G., Kim, D.W., Hwang, I.K., Choi, S.Y., Moon, S.M., 2018. Phosphatidylethanolamine-binding protein 1 protects CA1 neurons against ischemic damage via ERK-CREB signaling in Mongolian gerbils. Neurochem. Int. 118, 265–274.
Kaufman, R.J., 2002. Orchestrating the unfolded protein response in health and disease. J. Clin. Invest. 110, 1389–1398.
Kilkenny, C., Browne, W.J., Cuthill, I.C., Emerson, M., Altman, D.G., 2010. Improving bioscience research reporting: the ARRIVE guidelines for reporting animal research. PLoS Biol. 8, e1000412.
Kim, S.M., Hwang, I.K., Yoo, D.Y., Eum, W.S., Kim, D.W., Shin, M.J., Ahn, E.H., Jo, H.S., Ryu, E.J., Yong, J.I., Cho, S.W., Kwon, O.S., Lee, K.W., Cho, Y.S., Han, K.H., Park, J., Choi, S.Y., 2015. Tat-antioxidant 1 protects against stress-induced hippocampal HT-22 cells death and attenuate ischaemic insult in animal model. J. Cell Mol. Med. 19, 1333–1345.
Kozlov, G., Määttänen, P., Thomas, D.Y., Gehring, K., 2010. A structural overview of the PDI family of proteins. FEBS J. 277, 3924–3936.
Kozutsumi, Y., Segal, M., Normington, K., Gething, M.J., Sambrook, J., 1988. The presence of malfolded proteins in the endoplasmic reticulum signals the induction of glucose-regulated proteins. Nature 332, 462–464.
Kudo, T., Kanemoto, S., Hara, H., Morimoto, N., Morihara, T., Kimura, R., Tabira, T., Imaizumi, K., Takeda, M., 2008. A molecular chaperone inducer protects neurons from ER stress. Cell Death Differ. 15, 364–375.
Kumar, R., Krause, G.S., Yoshida, H., Mori, K., DeGracia, D.J., 2003. Dysfunction of the unfolded protein response during global brain ischemia and reperfusion. J. Cerebr. Blood Flow Metabol. 23, 462–471.

Lee, D.Y., Lee, K.S., Lee, J.H., Kim, D.H., Noh, Y.H., Yu, K., Jung, H.Y., Lee, S.H., Lee, J.Y., Youn, Y.C., Jeong, Y., Kim, D.K., Lee, W.B., Kim, S.S., 2010. Activation of PERK signaling attenuates Aβ-mediated ER stress. PloS One 5, e10489.
Linz, A., Knieper, Y., Gronau, T., Hansen, U., Aszodi, A., Garbi, N., Hämmerling, G.J., Pap, T., Bruckner, P., Dreier, R., 2015. ER stress during the pubertal growth spurt results in impaired long-bone growth in chondrocyte-specific ERp57 knockout mice. J. Bone Miner. Res. 30, 1481–1493.
Liu, H., Chen, J., Li, W., Rose, M.E., Shinde, S.N., Balasubramani, M., Uechi, G.T., Mutus, B., Graham, S.H., Hickey, R.W., 2015. Protein disulfide isomerase as a novel target for cyclopentenone prostaglandins: implications for hypoxic ischemic injury. FEBS J. 282, 2045–2059.
Liu, X., Wang, M., Chen, H., Guo, Y., Ma, F., Shi, F., Bi, Y., Li, Y., 2013. Hypothermia protects the brain from transient global ischemia/reperfusion by attenuating endoplasmic reticulum response-induced apoptosis through CHOP. PloS One 8, e53431.
Liu, Z., Wang, Y., Wang, Y., Dong, W., Xia, X., Song, E., Song, Y., 2017. Effect of subcellular translocation of protein disulfide isomerase on tetrachlorobenzoquinone-induced signaling shift from endoplasmic reticulum stress to apoptosis. Chem. Res. Toxicol. 30, 1804–1814.
Loskota, W.A., Lomax, P., Verity, M.A., 1974. A Stereotaxic Atlas of the Mongolian Gerbil Brain (*Meriones unguiculatus*). Ann Arbor Science Publishers Inc., Ann Arbor.
Määttänen, P., Gehring, K., Bergeron, J.J., Thomas, D.Y., 2010. Protein quality control in the ER: the recognition of misfolded proteins. Semin. Cell Dev. Biol. 21, 500–511.
Malhotra, J.D., Kaufman, R.J., 2007. Endoplasmic reticulum stress and oxidative stress: a vicious cycle or a double-edged sword? Antioxidants Redox Signal. 9, 2277–2293.
Matus, S., Valenzuela, V., Medinas, D.B., Hetz, C., 2013. ER dysfunction and protein folding stress in ALS. Int. J. Cell Biol. 2013, 674751.
McKracken, E., Graham, D.I., Nilsen, M., Stewart, J., Nicoll, J.A., Horsburgh, K., 2004. 4-Hydroxynonenal immunoreactivity is increased in human hippocampus after global ischemia. Brain Pathol. 11, 414–421.
Merksamer, P.I., Trusina, A., Papa, F.R., 2008. Real-time redox measurements during endoplasmic reticulum stress reveal interlinked protein folding functions. Cell 135, 933–947.
Nakamura, T., Lipton, S.A., 2009. Cell death: protein misfolding and neurodegenerative diseases. Apoptosis 14, 455–468.
Nakamura, T., Lipton, S.A., 2011. Redox modulation by S-nitrosylation contributes to protein misfolding, mitochondrial dynamics, and neuronal synaptic damage in neurodegenerative diseases. Cell Death Differ. 18, 1478–1486.
Noh, M.R., Kim, J.I., Han, S.J., Lee, T.J., Park, K.M., 2015. C/EBP homologous protein (CHOP) gene deficiency attenuates renal ischemia/reperfusion injury in mice. Biochim. Biophys. Acta 1852, 1895–1901.
Nomura, Y., 2004. Neuronal apoptosis and protection: effects of nitric oxide and endoplasmic reticulum-related proteins. Biol. Pharm. Bull. 27, 961–963.
Oida, Y., Shimazawa, M., Imaizumi, K., Hara, H., 2008. Involvement of endoplasmic reticulum stress in the neuronal death induced by transient forebrain ischemia in gerbil. Neuroscience 151, 111–119.
Oyadomari, S., Mori, M., 2004. Roles of CHOP/GADD153 in endoplasmic reticulum stress. Cell Death Differ. 11, 381–389.
Paz Gavilán, M., Vela, J., Castaño, A., Ramos, B., del Río, J.C., Vitorica, J., Ruano, D., 2006. Cellular environment facilitates protein accumulation in aged rat hippocampus. Neurobiol. Aging 27, 973–982.
Pekny, M., Wilhelmsson, U., Pekna, M., 2014. The dual role of astrocyte activation and reactive gliosis. Neurosci. Lett. 565, 30–38.
Pendyala, G., Ninemire, C., Fox, H.S., 2012. Protective role for the disulfide isomerase PDIA3 in methamphetamine neurotoxicity. PloS One 7, e38909.
Rao, R.V., Peel, A., Logvinova, A., del Rio, G., Hermel, E., Yokota, T., Goldsmith, P.C., Ellerby, L.M., Ellerby, H.M., Bredesen, D.E., 2002. Coupling endoplasmic reticulum stress to the cell death program: role of the ER chaperone GRP78. FEBS Lett. 514, 122–128.
Roberts, G.G., Di Loreto, M.J., Marshall, M., Wang, J., DeGracia, D.J., 2007. Hippocampal cellular stress responses after global brain ischemia and reperfusion. Antioxidants Redox Signal. 9, 2265–2275.
Rutkowski, D.T., Arnold, S.M., Miller, C.N., Wu, J., Li, J., Gunnison, K.M., Mori, K., Sadighi Akha, A.A., Raden, D., Kaufman, R.J., 2006. Adaptation to ER stress is mediated by differential stabilities of pro-survival and pro-apoptotic mRNAs and proteins. PLoS Biol. 4, e374.
Schröder, M., Kaufman, R.J., 2005. The mammalian unfolded protein response. Annu. Rev. Biochem. 74, 739–789.
Serve, O., Kamiya, Y., Maeno, A., Nakano, M., Murakami, C., Sasakawa, H., Yamaguchi, Y., Harada, T., Kurimoto, E., Yagi-Utsumi, M., Iguchi, T., Inaba, K., Kikuchi, J., Asami, O., Kajino, T., Oka, T., Nakasako, M., Kato, K., 2010. Redox-dependent domain rearrangement of protein disulfide isomerase coupled with exposure of its substrate-binding hydrophobic surface. J. Mol. Biol. 396, 361–374.
Severino, A., Campioni, M., Straino, S., Salloum, F.N., Schmidt, N., Herbrand, U., Frede, S., Toietta, G., Di Rocco, G., Bussani, R., Silvestri, F., Piro, M., Liuzzo, G., Biasucci, L.M., Mellone, P., Feroce, F., Capogrossi, M., Baldi, F., Fandrey, J., Ehrmann, M., Crea, F., Abbate, A., Baldi, A., 2007. Identification of protein disulfide isomerase as a cardiomyocyte survival factor in ischemic cardiomyopathy. J. Am. Coll. Cardiol. 50, 1029–1037.
Shibata, M., Hattori, H., Sasaki, T., Gotoh, J., Hamada, J., Fukuuchi, Y., 2003. Activation of caspase-12 by endoplasmic reticulum stress induced by transient middle cerebral artery occlusion in mice. Neuroscience 118, 491–499.
Shin, M.J., Kim, D.W., Lee, Y.P., Ahn, E.H., Jo, H.S., Kim, D.S., Kwon, O.S., Kang, T.C., Cho, Y.J., Park, J., Eum, W.S., Choi, S.Y., 2014. Tat-glyoxalase protein inhibits against ischemic neuronal cell damage and ameliorates ischemic injury. Free Radic. Biol. Med. 67, 195–210.
Sohn, E.J., Shin, M.J., Eum, W.S., Kim, D.W., Yong, J.I., Ryu, E.J., Park, J.H., Cho, S.B., Cha, H.J., Kim, S.J., Yeo, H.J., Yeo, E.J., Choi, Y.J., Im, S.K., Kweon, H.Y., Kim, D.S., Yu, Y.H., Cho, S.W., Park, M., Park, J., Cho, Y.J., Choi, S.Y., 2016. Tat-NOL3 protects against hippocampal neuronal cell death induced by oxidative stress through the regulation of apoptotic pathways. Int. J. Mol. Med. 38, 225–235.
Song, J., Zhang, Y., Zhang, W., Chen, J., Yang, X., Ma, P., Zhang, B., Liu, B., Ni, J., Wang, R., 2015. Cell penetrating peptide TAT can kill cancer cells via membrane disruption after attachment of camptothecin. Peptides 63, 143–149.
Srimanee, A., Regberg, J., Langel, Ü., 2015. Application of CPPs for brain delivery. Methods Mol. Biol. 1324, 349–356.
Suzuki, R., Yamaguchi, T., Li, C.L., Klatzo, I., 1983. The effects of 5-minute ischemia in Mongolian gerbils: II. Changes of spontaneous neuronal activity in cerebral cortex and CA1 sector of hippocampus. Acta Neuropathol. 60, 217–222.
Tajiri, S., Oyadomari, S., Yano, S., Morioka, M., Gotoh, T., Hamada, J.I., Ushio, Y., Mori, M., 2004. Ischemia-induced neuronal cell death is mediated by the endoplasmic reticulum stress pathway involving CHOP. Cell Death Differ. 11, 403–415.
Tanaka, S., Uehara, T., Nomura, Y., 2000. Up-regulation of protein-disulfide isomerase in response to hypoxia/brain ischemia and its protective effect against apoptotic cell death. J. Biol. Chem. 275, 10388–10393.
Tikka, T., Fiebich, B.L., Goldsteins, G., Keinanen, R., Koistinaho, J., 2001. Minocycline, a tetracycline derivative, is neuroprotective against excitotoxicity by inhibiting activation and proliferation of microglia. J. Neurosci. 21, 2580–2588.
Truettner, J.S., Hu, K., Liu, C.L., Dietrich, W.D., Hu, B., 2009. Subcellular stress response and induction of molecular chaperones and folding proteins after transient global ischemia in rats. Brain Res. 1249, 9–18.
Uehara, T., Nakamura, T., Yao, D., Shi, Z.Q., Gu, Z., Ma, Y., Masliah, E., Nomura, Y., Lipton, S.A., 2006. *S*-nitrosylated protein-disulphide isomerase links protein misfolding to neurodegeneration. Nature 441, 513–517.
Wang, C., Li, W., Ren, J., Fang, J., Ke, H., Gong, W., Feng, W., Wang, C.C., 2013. Structural insights into the redox-regulated dynamic conformations of human protein disulfide isomerase. Antioxidants Redox Signal. 19, 36–45.
Wang, Q., Tompkins, K.D., Simonyi, A., Korthuis, R.J., Sun, A.Y., Sun, G.Y., 2006. Apocynin protects against global cerebral ischemia-reperfusion-induced oxidative stress and injury in the gerbil hippocampus. Brain Res. 1090, 182–189.
Yoo, D.Y., Cho, S.B., Jung, H.Y., Kim, W., Choi, G.M., Won, M.H., Kim, D.W., Hwang, I.K., Choi, S.Y., Moon, S.M., 2017. Tat-protein disulfide-isomerase A3: a possible candidate for preventing ischemic damage in the spinal cord. Cell Death Dis. 8, e3075.
Yoo, D.Y., Jung, H.Y., Nam, S.M., Kim, J.W., Choi, J.H., Kwak, Y.G., Yoo, M., Lee, S., Yoon, Y.S., Hwang, I.K., 2015. *Valeriana officinalis* extracts ameliorate neuronal damage by suppressing lipid peroxidation in the gerbil hippocampus following transient cerebral ischemia. J. Med. Food 18, 642–647.
Yuan, G., Hua, B., Cai, T., Xu, L., Li, E., Huang, Y., Sun, N., Yan, Z., Lu, C., Qian, R., 2017a. Clock mediates liver senescence by controlling ER stress. Aging (N Y) 9, 2647–2665.
Yuan, G., Hua, B., Yang, Y., Xu, L., Cai, T., Sun, N., Yan, Z., Lu, C., Qian, R., 2017b. The circadian gene clock regulates bone formation via PDIA3. J. Bone Miner. Res. 32, 861–871.
Zhang, G.X., Li, J., Ventura, E., Rostami, A., 2002. Parenchymal microglia of naïve adult C57BL/6J mice express high levels of B7.1, B7.2, and MHC class II. Exp. Mol. Pathol. 73, 35–45.
Zhao, G., Lu, H., Li, C., 2015a. Proapoptotic activities of protein disulfide isomerase (PDI) and PDIA3 protein, a role of the Bcl-2 protein Bak. J. Biol. Chem. 290, 8949–8963.
Zhao, Y., Yan, Y., Zhao, Z., Li, S., Yin, J., 2015b. The dynamic changes of endoplasmic reticulum stress pathway markers GRP78 and CHOP in the hippocampus of diabetic mice. Brain Res. Bull. 111, 27–35.